Since January 2020 Elsevier has created a COVID-19 resource centre with free information in English and Mandarin on the novel coronavirus COVID-19. The COVID-19 resource centre is hosted on Elsevier Connect, the company's public news and information website.

ELSEVIER

Biophysical Chemistry 112 (2004) 15–25

Biophysical Chemistry

www.elsevier.com/locate/bpc

In vitro biochemical and thermodynamic characterization of nucleocapsid protein of SARS

Haibin Luo[a,b], Fei Ye[a,b], Tao Sun[a,b], Liduo Yue[a,b], Shuying Peng[a,b], Jing Chen[a], Guowei Li[a], Yi Du[a], Youhua Xie[c], Yiming Yang[a], Jianhua Shen[a], Yuan Wang[c], Xu Shen[a,*], Hualiang Jiang[a,*]

[a]*Drug Discovery and Design Center, State Key Lab of Drug Research, Shanghai Institute of Materia Medica, Shanghai Institutes for Biological Sciences, Chinese Academy of Sciences, Shanghai 201203, China*
[b]*Graduate School of the Chinese Acadamy of Sciences, Chinese Academy of Sciences, Shanghai, China*
[c]*Shanghai Institute of Biochemistry and Cell Biology, Shanghai Institutes for Biological Sciences, Chinese Academy of Sciences, Shanghai 200031, China*

Received 27 May 2004; received in revised form 23 June 2004; accepted 23 June 2004
Available online 20 July 2004

Abstract

The major biochemical and thermodynamic features of nucelocapsid protein of SARS coronavirus (SARS_NP) were characterized by use of non-denatured gel electrophoresis, size-exclusion chromatographic and surface plasmon resonance (SPR) techniques. The results showed that SARS_NP existed in vitro as oligomer, more probably dimer, as the basic functional unit. This protein shows its maximum conformational stability near pH 9.0, and it seems that its oligomer dissociation and protein unfolding occur simultaneously. Thermal-induced unfolding for SARS_NP was totally irreversible. Both the thermal and chemical denaturant-induced denaturation analyses showed that oligomeric SARS_NP unfolds and refolds through a two-state model, and the electrostatic interactions among the charge groups of SARS_NP made a significant contribution to its conformational stability.

Keywords: SARS; Nucleocapsid protein; SPR; Circular dichroism; Fluorescence; Protein folding and unfolding

1. Introduction

Between the end of the year 2002 and the June of the year 2003, one severe epidemic disease called severe acute respiratory syndrome (SARS) broke out in China and more than 30 other countries. It has been known that SARS coronavirus (SARS_CoV) is a novel human coronavirus and responsible for SARS infection [1–4]. Recently, remarkable achievements have been made in genome sequencing of SARS_CoV [5], SARS protein functional studies [6–8], three-dimensional structural modeling [9–11], and X-ray crystal structural analysis [12].

SARS_CoV genome contains 11 major open reading frames (ORFs) that encode the replicase polyprotein, the spike (S) protein, the small envelope (E) protein, the membrane (M) protein, and the nucleocapsid protein (NP) [5]. For coronaviruses, NP plays an important role in the host cell entry and virus particle assembly and release [13–15]. In particular, it binds to a defined packaging signal of viral RNA, leading to the formation of the helical nucleocapsid. NP is incorporated into virions by intracellular budding through a membrane containing three envelope proteins: the M glycoprotein [15], the E protein and S glycoprotein [16]. Additionally, NP has been

Abbreviations: SARS_CoV, severe acute respiratory syndrome coronavirus; SARS_NP, nucleocapsid protein of SARS; SPR, surface plasmon resonance; GuHCl, guanidine hydrochloride; CD, circular dichroism; T_m and C_m, transition midpoints of thermal and chemical denaturations; IPTG, isopropyl-β-D-thiogalasctopyranoside; N and U, native and unfolded states.

* Corresponding author. Tel.: +86 21 50807188; fax: +86 21 50807088.
E-mail addresses: xshen@mail.shcnc.ac.cn (X. Shen), hljiang@mail.shcnc.ac.cn (H. Jiang).

0301-4622/$ - see front matter © 2004 Elsevier B.V. All rights reserved.
doi:10.1016/j.bpc.2004.06.008

proposed to be multifunctional with additional roles in replication, transcription and translation for coronaviruses [17–19].

To our knowledge, nucleocapsid protein (NP) of some kinds of viruses might self-assemble as oligomer when carrying out its biological functions [19–21]. While we are preparing this manuscript, Surjit et al. [22] published their result that SARS_NP is capable of self-association through a C-terminal 209-amino-acid interaction domain, even though there is lack of detailed description for this work. Additionally, Jaenicke and Seckler [23] reported that oligomeric proteins always form intermediate and give more than one transition during unfolding. Nevertheless, whether NP forms intermediate during unfolding has not yet been reported elsewhere. In this report, we used non-denatured gel electrophoresis and size-exclusion chromatographic techniques as well as surface plasmon resonance (SPR) technology based Bicore3000 for trying to investigate quantitatively the possible assembly features of SARS_NP. The results suggested that in the absence of genomic nucleic acid, SARS_NP tends to form dimer at a low concentration, and trimer or polymer at higher concentration. In addition, the unfolding and refolding characterizations of SARS_NP dimer caused by thermal- and chemical denaturant-induced denaturations were also inspected by fluorescent and CD spectral investigation, it is found that SARS_NP exhibits its most stable conformation near pH 9.0, and its oligomer dissociation and protein unfolding seem to be of coinstantaneous occurring events.

2. Materials and methods

2.1. Materials and SARS_NP plasmid

The restriction and modifying enzymes were purchased from TaKaRa, and the vector pQE30, the bacterial strains M15 and DH5α were from Qiagen. TRIzol and Superscript II reverse transcriptase were bought from GIBCO. Trypsin (sequencing grade) was purchased from Sigma. DNAase and RNAase were from NEB. The chelating affinity column and lower molecular weight (LMW) marker and ovalbumin (45 kDa) used as gel filtration reference protein were purchased from Amersham Pharmacia Biotech (Sweden). All other chemicals were from Sigma in analytical grade.

All cloning techniques including PCR, restriction digestion, ligation, *Escherichia coli* transformation, plasmid DNA preparation, were according to the literature method [24].

SARS_CoV (isolate BJ01) RNA was extracted with TRIzol reagent according to the manufacturer's instruction (http://www.genehub.net/trizol.htm). The reverse transcription was performed with the random priming method by the Superscript II reverse transcriptase.

The appropriate SARS_NP coding sequence (TRO2) was isolated by PCR from the cDNA of SARS_CoV. The obtained SARS_NP DNA was amplified by PCR using the primers:

NPf,
5′ATTAGGATCCTCTGATAATGGACCCCAATCA 3′;
NPr,
5′ TTAAGTCGACTGCCTGAGTTGAATCAGCAGA 3′.

The PCR products were digested by *Bam*HI and *Sal*I restriction enzymes then inserted into the pQE30 vector (QIAgen). The construct of pQE30-SARS_NP was sequenced.

2.2. Expression and purification of SARS_NP

The recombinant plasmid pQE30-SARS_NP was transfected into M15 (DE3) bacterial strain. Clones were grown overnight in LB medium containing 100 mg/l ampicillin and 25 mg/l kanamycin. Expression of the His-tagged recombinant protein (SARS_NP) was induced at an OD_{600} of 0.7–0.9 with the addition of isopropyl-β-D-thiogalasctopyranoside (IPTG) to a final concentration of 1 mM. After induction for 12 h at 37 °C, the cells were harvested by centrifugation for 30 min at 4000 rpm, 4 °C and stored at −70 °C. During the protein purification, cells were resuspended in 20 ml of buffer A (20 mM Tris–HCl, pH 8.0, 500 mM NaCl, 5 mM imidazole, 1 mM PMSF), and then lysed by sonication for 15 min in ice bath. The lysate was cleared by centrifugation at 4 °C, 14000 rpm for 60 min. To the supernatant were added DNAase and RNAase to the final concentration of 2 μg/ml for either of them in order to get rid of the possible bound DNA and RNA scraps to the protein of interest. This mixture was incubated at 20 °C for 3 h before further treatments.

The nuclease treated supernatant was loaded on a 4 ml of Sepharose Ni-NTA column (Amersham Pharmacia) equilibrated with 30 ml of buffer A. The column was eluted with buffer B (20 mM Tris–HCl, pH 8.0, 500 mM NaCl, 500 mM imidazole) after being washed by buffer C (20 mM Tris–HCl, pH 8.0, 500 mM NaCl, 120 mM imidazole). The elution fraction was further applied to a gel filtration column (HiprepTM 16/60 sephacyl S100) on a FPLC (Amersham Pharmacia) system. The column was pre-equilibrated with 2 column volumes of Buffer D (20 mM Tris–HCl, pH 8.0, 150 mM NaCl, 1.5 mM EDTA) before loading the protein sample (2 ml). SARS_NP was thus eluted by 1.5 column volumes of Buffer D, and concentrated by Centricon (Pharmacia) The protein purity was determined by SDS-PAGE and concentration was monitored by measuring the absorbance at 280 nm in Buffer D using the extinction coefficient of 43,890 l/mol/cm. SARS_NP sequence was confirmed through LC-Ion Trap-MS and MS/Ms techniques.

2.3. Surface plasmon resonance (SPR) analysis

SARS_NP/SRAS_NP interaction analysis was performed using the dual flow cell Biacore 3000 instrument (Biacore, Rapsgatan 7, S-754 50 Uppsala, Sweden). All the experiments were carried out at a constant system flow rate of 20 μl/min at 25 °C. SARS_NP was immobilized on a CM5 sensor chip by amine coupling at the level of 4000 response units (RU). In considering that this signal may involve the SARS_NP oligomer (as stated in later related parts), several injections of 10 μl of 100 mM NaOH were processed in order to wash out the possible oligomers of SRAS_NP as completely as possible. The next injection was performed after the stable response unit (around 2400 RU in this stage) was obtained. The reference flow cell surface was immobilized at a parallel level (2200 RU) using lysozyme. Every sample injection was performed at 30 μl/min within 1 min and the surface was regenerated by injection of 10 μl of 100 mM NaOH twice.

2.4. Fluorescence and circular dichroism (CD) spectral investigations

Fluorescent spectra were recorded on a HITACHI F-2500 fluorescence spectrophotometer in a 1-cm quartz cell. For monitoring tryptophan fluorescence excitation, wavelength of 285 nm was used, and the spectra were collected between 300 and 400 nm. Both the excitation and emission slits were 5 nm.

CD spectra were recorded on a JASCO J810 spectropolarimeter calibrated with ammonium (+)-10-camphorsulfonate, and normalized by subtracting the baseline recorded for the buffer having the same concentration of denaturant under similar conditions.

2.5. Thermal and chemical denaturant-induced denaturations

Equilibrium unfolding experiments were performed in 20 mM Tris–HCl, 150 mM NaCl, 1.5 mM EDTA, pH 6.0–11.0 with the protein concentration at 0.4–4.0 μM (0.2–2 mg/ml). Thermal denaturations were characterized with the help of intrinsic fluorescence and far-UV CD (λ=222 nm) spectral investigations. The temperature was scanned in a 5° interval from 20 to 95 °C heated by a thermostat. Each measurement was repeated three times and the final result was the average.

Protein samples were incubated in the presence of 0–8 M urea (or 0–6 M GuHCl) for at least 12 h at 16 °C prior to fluorescence and CD measurements. Urea stock solution in 9 M was made freshly for each experiment, and GuHCl stock solution in 8 M was used within 1 week.

The chemical denaturant-induced denaturations in urea and GuHCl were performed in Buffer D (pH 9.0) at 25 °C. For each experiment, a known amount of buffer was mixed with a fixed amount of the protein stock solution and varying amounts of the denaturant in a final volume of 2 ml, and the final signal was obtained by subtracting the same concentration of the denaturant buffer.

2.6. SARS_NP refolding analysis

During the protein refolding experiment from thermal-induced denatured state, the samples heated to different temperatures (30–95 °C) were cooled down to 25 °C, and kept at this temperature for 12 h, then applied to the refolding analysis by fluorescence and CD instruments at 25 °C.

While in the refolding test from the chemical denaturant-induced denatured state, protein samples were incubated at 16 °C for 12 h with denaturant in different concentrations (0–8 M for urea; 0–6 M for GuHCl). The sample was dialyzed against Buffer D at 16 °C for 24 h, and then left to stand still for 1 h at 25 °C before fluorescence and CD spectral investigations.

2.7. Size-exclusion chromatography assay

Gel filtration experiments were carried out on a HiprepTM16/60 Sephacyl S100 column on an AKTA FPLC (Amersham Pharmacia Biotech) system. The column was equilibrated and run with Buffer D at 20 °C. At the same temperature, 2 ml of protein sample was loaded on the column and run in a flow rate of 0.5 ml/min with a detection of 280 nm absorbance. Two proteins, GST-PPARα-LBD (90 kDa) and ovalbumin (45 kDa) were used as references. GST-PPARα-LBD was expressed and purified in our lab according to the published method by Xu et al. [25].

2.8. BIAcore data analysis

Response curves were prepared by subtraction of the signal generated simultaneously on the control flow cell. As will be discussed in the later part, the binding feature for SARS_NP/SARS_NP characterized as a complex mode with (A+B↔AB; AB+A↔AB; AA+B↔AAB), which thus cannot be simply fitted by BIAevalation binding model. However, according to the formula:

$$R_{\max} = \frac{MW_{\text{analyte}}}{MW_{\text{ligand}}} \times R_{\text{coupled}} \times \text{stoichiometry} \quad (1)$$

We can follow the response unit (RU) value to quantify approximately the protein concentration where SARS_NP formed dimer or higher order oligomer. At the same time, the slope of the affinity curve may be used to characterize the association and dissociation features.

2.9. Thermal-induced denaturation data analysis

Data from fluorescence and CD measurements were fitted as non-linear least-squares regression to the following equation for a typical two-state transition [26,27]

$$Y = \frac{(Y_n + M_n T) + (Y_d + M_d T)\{\exp[\Delta H_m / R(1/T_m - 1/T)]\}}{1 + \exp[\Delta H_m / R(1/T_m - 1/T)]} \quad (2)$$

where Y is the experimental data (the fluorescent intensities at 340 nm, or fluorescent maximum emission λ_{max} shifts, or the ellipticity values at 222 nm in CD), T is the temperature in Kevin, R is the gas constant (1.987×10^{-3} kcal/mol), T_m is the transition temperature, and ΔH_m is the enthalpy of unfolding at T_m (van't Hoff enthalpy). The parameters Y_n and Y_d refer to the Y intercepts of the native and denatured baseline, respectively, while M_n and M_d are the slopes of the baselines. These raw experimental data were fitted to the Eq. (2) using Origin 6.0 (OriginLab, http://www.OriginLab.com).

To compare the transitions monitored at different concentrations, each unfolding curve was normalized to the apparent fraction of the unfolded form by using the following relations [27]:

$$f_u = \frac{y - Y_n}{Y_d - Y_n} \quad (3)$$

In Eq. (3), y is the value of the optical parameter being monitored, Y_n and Y_d are the values for the fully folded and fully unfolded state at each temperature as determined by linear regression of the points in the unfolding experiments.

Data from thermal and chemical denaturant-induced denaturation experiments at different pH values ranging from 6.0 to 11.0 were used to construct a plot of ΔH_m versus T_m. The slope of this plot (ΔC_p, heat capacity) was determined by linear least-squares fitting according to the following equation [27].

$$\Delta H_m = \Delta C_p(T_m) + B \quad (4)$$

Thermodynamic parameters T_m and ΔH_m, obtained from the spectroscopic measurements, were used to figure out the free energy changes (ΔG°) of unfolding at temperature (T) by using the following Gibbs–Helmholtz equation [27]:

$$\Delta G^\circ(T) = \Delta H_m(1 - T/T_m) - \Delta C_p[(T_m - T) + T\ln(T/T_m)] \quad (5)$$

where T is the absolute temperature. The entropy change (ΔS_m) of unfolding was determined by following equation [27,28]:

$$\Delta S_m = \frac{\Delta H_m}{T} \quad (6)$$

2.10. Chemical denaturant-induced denaturation data analysis

The apparent free energy change ($\Delta G_u^{H_2O}$) in the absence of denaturant was determined by fitting the optical value changes at a particular concentration of denaturant to the following equation [29]:

$$Y = \frac{(Y_n + S_n[D]) + (Y_d + S_d[D])\exp\left[\left(m[D] - \Delta G_u^{H_2O)}\right)/RT\right)}{1 + \exp\left[\left(m[D] - \Delta G_u^{H_2O}\right)/RT\right]} \quad (7)$$

where Y is the experimental data (the fluorescent intensities at 340 nm, or fluorescent maximum emission λ_{max} shifts, or the ellipticity values at 222 nm in CD), [D] is the denaturant concentration in molar (M), Y_n and S_n are the slope and intercept of the denaturant-free native state baseline, Y_d and S_d are the slope and the intercept of denaturant induced fully denatured state baseline, and m stands for the slope of the linear free energy denaturant dependence. The raw data were fitted by non-linear least squares regression analysis using Origin 6.0 (OriginLab, http://www.OriginLab.com).

3. Results and discussion

3.1. Assembly characterization

The purified His-tagged SARS_NP was isolated through a nickel metal-affinity column followed by a gel filtration column on an FPLC system. The purity (>95%) of SARS_NP was examined by SDS-PAGE with one single band corresponding to 48 kDa. Otherwise, LC/MS and LC/MS/MS analyses were processed for protein identity determination (see Supplementary materials).

It has been known that nucleocapsid protein (NP) of many kinds of viruses tend to self-assemble with genomic nucleic acid for implementation of their biological functions [19,30,31]. For example, for NP of hepatitis B virus, its assembly does not occur without genomic DNA in vivo [19,30,32], and few cases about NP self-assembly without RNA/DNA in vitro were reported [33,34]. Surjit et al. [22] recently expressed the N protein as a fusion protein in the yeast two-hybrid system to demonstrate self-association and confirmed dimerization of the N protein from mammalian cell lysates by coimmunoprecipitation. However, SARS_NP self-assembly as higher order oligomers in the absence of genomic RNA in vitro was observed in our present work.

To preliminarily study the self-assembly of SAS_NP, non-denatured gel electrophoresis technique was applied. The result was shown in Fig. 1A, where the protein (0.5 mg/ml) was mixed with 4 M urea, then used as a reference for monomer on native gel. It is found that at its low concentration around 1.0 mg/ml, SARS_NP tends to form largely in monomer involving a small quantity of dimer

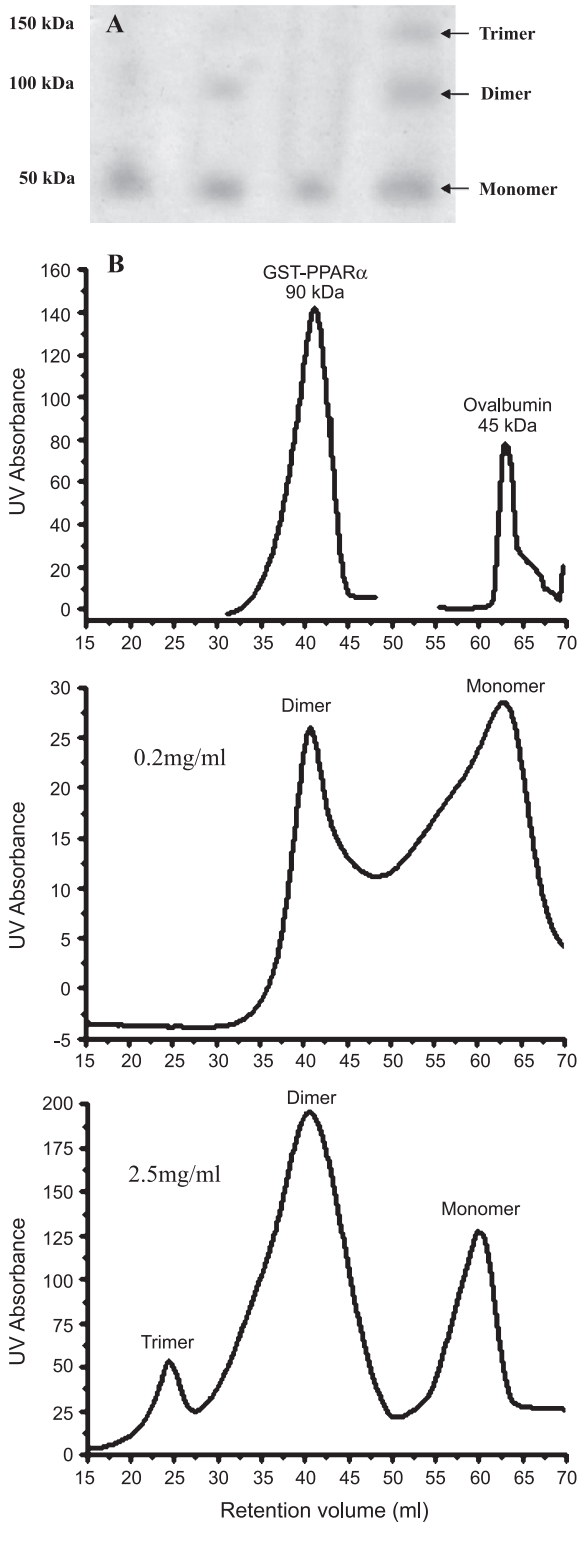

Fig. 1. Oligomerization of SARS_NP as a function of concentration. (A) Different concentrations of SARS_NP run in 6% native gel (electrophoresis buffer, pH 9.0, lanes are numbered from left to right sequentially) were visualized by Coomasie brilliant blue: lane 1, 1 mg/ml; lane 2, 1.5 mg/ml; lane 3, 1.5 mg/ml in 4 M urea; lane 4, 3.0 mg/ml. (B) Size-exclusion chromatography on a gel filtration S100 16/60 column in FPLC system at 20 °C. The loaded volume of 2 ml was for each sample. GST-PPAR-α (81 kDa, 4 mg/ml) and ovalbumin (45 kDa, 0.5 mg/ml) were used as reference protein.

(Lane 1), and the amount of dimer is fortified with the increasing concentration of SARS_NP (~1.5 mg/ml) as indicated in lane 2. When the protein concentration was higher (~3.0 mg/ml), the trimer state of SARS_NP appeared (Lane 4). Such a result suggested that homo-oligomerization of SARS_NP is of concentration dependence. Due to the difficulty in obtaining large quantity of soluble SARS_NP and the weak visualization of Coomassie brilliant blue dye for SARS_NP in gel, higher polymer than trimer could not be obtained for SARS_NP by native gel.

In order to gain more insight into the assembly mechanism for SARS_NP, and evaluate the molecular dimensions of the native SARS_NP dependence on concentration, size-exclusion chromatographic studies on an S100 gel filtration column were carried out according to the published method [21]. The two reference proteins GST-PPARα (90 kDa) and ovalbumin (45 kDa) with the elution peaks at 42.3 and 63.1 ml (Fig. 1B), respectively, were used for molecular weight indication in size-exclusion chromatographic experiment.

As also indicated in Fig. 1B, some more detailed interesting results could be also found: For SARS_P at 0.2 mg/ml, two elution peaks emerged at 40.7 and 61.8 ml. According to the reference proteins, these two peaks might be ascribed to the dimer and monomer of SARS_NP, respectively; SARS_NP at 2.5 mg/ml had a new small elution peak at 23.8 ml, which may be ascribed to SARS_NP trimer. This is in agreement with the results of non-denatured gel electrophoresis that oligomer formation of SRAS_NP is of concentration dependence. According to Fig. 1B, SARS_NP at 0.2 mg/ml contained equivalent ratio of monomer and dimer, and at 2.5 mg/ml, it existed as a mixture with more dimer and less monomer and trimer. It is noticed that in native gel experiment, SARS_NP at different concentrations existed mostly in monomer state. This might be resulted from the experimental differences between native gel and gel filtration. The heat generated during the native gel test might cause some of the protein oligomer to dissociate into monomer.

As reflected in the amino acid sequence of SARS_NP, there is no cysteine residue in the structure of SARS_NP, its polymerization as oligomer was thus probably be attributed to the non-covalently bond forces, different from the oligomerization feature for NP of porcine reproductive and respiratory syndrome virus whose oligomers formation involves disulfide linkage [35].

SPR technology might be not highly competent for studying protein oligomerization in this report, but we can use it to qualitatively investigate SARS_NP protein oligomerization. To avoid the non-specific interactions, an equivalent amount of lysozyme was immobilized on the sensor chip as a reference. As shown in Fig. 2, even under very low concentrations (below 4 μM or 0.2 mg/ml), SARS_NP has tendency to assemble as dimer based on the fact that the binding curves in the sensor gram showed saturation tendency at 2000 RU, nearly equivalent to the

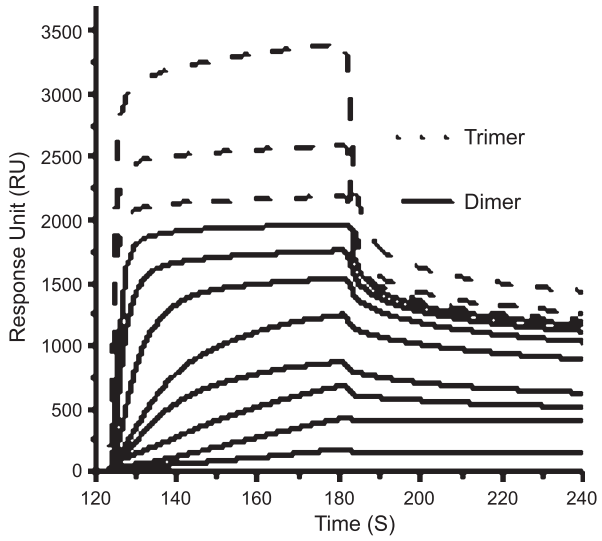

Fig. 2. SARS_NP/SARS_NP interactions studied by Biacore3000. Injections of different concentrations of SARS_NP at pH 8.0. From top to bottom: 32 μM, 16 μM, 8 μM, 4 μM, 2 μM, 1 μM, 500 nM, 250 nM, 117 nM, 58.6 nM and 29.3 nM. All data were obtained at 25 °C.

coupling level of 2400 RU. This result is in accordance with the fact obtained in size-exclusion chromatography experiment that SARS_NP exists as oligomer at 0.2 mg/ml. Furthermore, as indicated in Fig. 2, when SARS_NP concentration was higher than 4 μM (0.2 mg/ml), the binding level exceeded the immobilized one (2400 RU) on the sensor chip and increased in a linear way; this may be tentatively attributed to the formation of trimer (or higher polymer) for SRAS_NP. Therefore, based on the results from the non-denatured gel, gel filtration analyses and the preliminary SPR data, it is suggested that SARS_NP might exist in oligomer, more probably dimer, as the basic functional unit in vivo. As can be seen from Fig. 2 (dotted curves), the trimer (or higher polymer) of SARS_NP departed quickly firstly then appeared as the similar dissociation course to that of dimer, suggesting that during the dissociation course of SARS_NP oligomer, it firstly dissociates into dimer. The quicker dissociation course indicates that the structure of SARS_NP polymer is possibly less compact than that of its dimer.

It is suggested here that SARS_NP tends to form dimer and oligomer in vitro, and the order of oligomer increases with the protein concentration increasing. The polymerization of SARS_NP was thus surely driven totally by the non-covalently bond forces not the covalent ones.

3.2. pH-induced unfolding

The fluorescent and CD spectra with pH ranging from 3.5 to 12 for SARS_NP were monitored at room temperature for investigating its pH-induced denaturation. It is found that from pH 7.0 to 10.0, all the fluorescent intensities kept at high level with small changes, and far-UV CD measurements gave the similar spectra (Fig. 3A and B). From pH 10.5 to 12, the fluorescent intensity decreases dramatically with increase of pH value, and within the pH range between 3.5 and 6.0, the intensity decreased as the pH value increased. The emission λ_{max} maintained the value at 333 nm within pH values between 7.0 and 10.0, and changed to 336 nm at pH 11.0, then shifted to 345 nm above pH 11.5. These results suggested that SARS_NP lost its native structure at extreme pH. Additionally, at the extreme alkaline pH above 11.5, SARS_NP displayed a fluorescent spectrum similar to its thermal-induced and chemical denaturant-induced denaturations states (Fig. 5A). The far-UV CD spectra at pH>11.5 showed a typical random coil curve corresponding to the denatured protein of SARS_NP.

3.3. Thermal-induced denaturation

The thermal-induced denaturations of SARS_NP at various pH values were investigated by following the intrinsic fluorescence of SARS_NP and far-UV CD (at 222 nm) spectral analyses. Despite the fact that the unfolding of an oligomeric protein is dependent on the protein concentrations [36], this present work however showed the similar unfolding

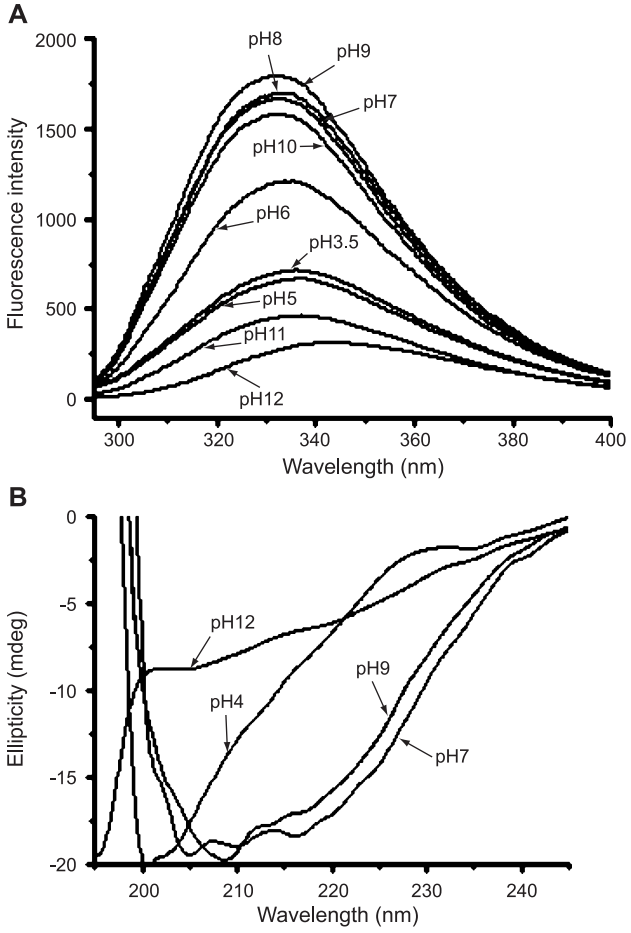

Fig. 3. pH-dependent unfolding of SARS_NP. Fluorescent spectra (A) and far-UV CD spectra (B) of SARS_NP in Buffer D (pH 3.5–12) at 25 °C. The numbers represent the pH values of protein solution. Protein concentrations used in fluorescent and CD measurements were 3.5 and 10 μM.

profiles for SARS_NP within the concentrations ranging from 1 to 6 μM (data not shown). Fig. 4A and B shows the typical fluorescence and far-UV CD spectral changes for thermal-induced denaturations of SARS_NP (SARS_NP concentration: 0.15 mg/ml for fluorescent experiment, and 0.45 mg/ml for CD). The changes in the fluorescent spectra and the well-fitted curves (according to Eq. (2)) showed related profiles (Fig. 4C). The fluorescent intensity was found to decrease with increase of temperature accompanied by a shift in emission λ_{max} from 333 to 343 nm (Fig. 4A and C), whereas far-UV CD spectral information suggested the loss of secondary structure for SARS_NP during its thermal-induced denaturation (Fig. 4B and D).

The denaturation curves studied by fluorescent intensity, emission λ_{max} and far-UV CD at 222 nm were analyzed using Eq. (2) (The fitting goodness was shown in Fig 4C and D), and ΔH_m was plotted against T_m (transition midpoint of thermal-induced denaturation) to obtain ΔC_p by linear fitting (Fig. 4E) (Eq. (4)). The averaged ΔC_p of 1.5039±0.0567 kcal/mol was used to calculate ΔG° (Eq. (5)), and the entropy changes (ΔS_m) (Eq. (6)) at different pH values. It was found that SARS_NP is more stable in alkaline than in acidic condition, indicating that the variation of the electric charge of the protein with pH change will modify the intra-molecular cooperative process [37].

Table 1 summarizes the thermodynamic parameters for characterizing the thermal denaturation of SARS_NP by fluorescence intensity, emission λ_{max} and CD ellipticity at 222 nm at different pH. In the pH ranges from 6.0 to 9.0, T_m increases with the increasing pH, e.g. from 42 °C at pH 6.0 to 48 °C at pH 9.0. However, T_m decreases with increasing pH after 9.0. The free energy (ΔG°) of unfolding is used to estimate the protein stability in enduring the denaturants, high ΔG° means the protein might be more stable against denaturant [28]. Comparing

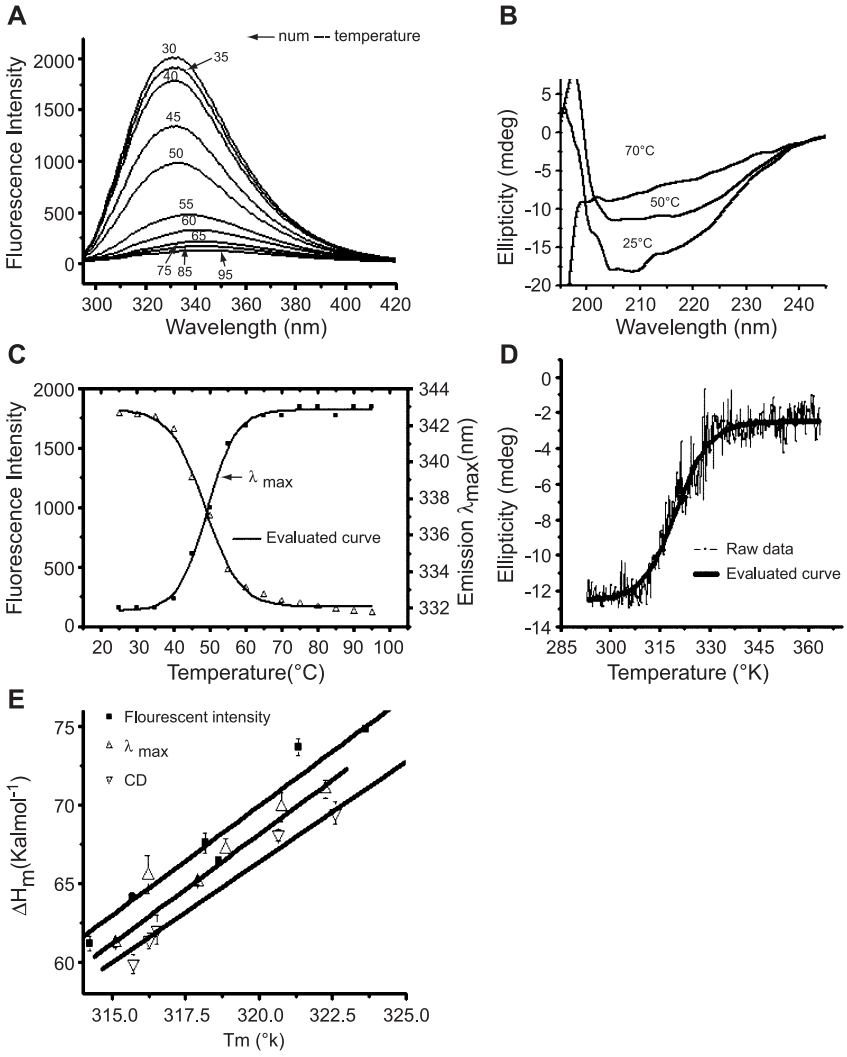

Fig. 4. Thermal-induced unfolding of SARS_NP. Fluorescent (A) and far-UV CD spectra (B) of SARS_NP (pH 9.0) at different temperatures with their fluorescence intensity (at 340 nm) and λ_{max} shifts (C) and $\Delta\theta$sub 222 (D). The solid curves in (C) and (D) show goodness of fitting by Eq. (2). ΔC_p value was obtained and averaged from the plots of ΔH_m versus T_m by three methods (E). Protein concentration used in fluorescent experiment was 0.15 mg/ml, and CD 0.45 mg/ml. All samples were prepared in Buffer D (pH 6.0–11).

Table 1
Thermodynamic parameters for the thermal denaturation of SARS_NP[a]

pH	Fluorescence				CD		ΔS_m (kcal/M)[b]	ΔG° (kcal/M)[b]
	Intensity		λ_{max}		$\theta_{222\ nm}$			
	T_m (K)	ΔH_m (kcal/M)	T_m (K)	ΔH_m (kcal/M)	T_m (K)	ΔH_m (kcal/M)		
6.0	314.24	70.21	315.12	68.24	315.73	59.92	0.215	2.498
7.0	315.70	64.15	316.21	65.578	316.53	62.07	0.202	2.874
8.0	318.61	66.49	318.88	67.211	320.67	68.11	0.223	3.336
9.0	323.63	74.85	322.28	71.052	326.38	71.67	0.251	4.459
10.0	321.35	73.70	320.77	69.885	322.61	69.51	0.247	4.126
11.0	318.17	62.50	317.9	62.153	316.27	61.39	0.223	3.288

[a] The values represent the mean of three independent sets of experiments with S.D. of less than 10%.
[b] ΔS_m and ΔG were calculated according to the fluorescent intensity.

the ΔG° values of SARS_NP at different pH, the conformational stability of SARS-NP is highest near pH 9.0, with the highest ΔG° about 4.459 kcal/mol.

3.4. Chemical denaturant-induced denaturation

Chemical denaturant-induced denaturations of SARS_NP were studied based on the totally measured tryptophan fluorescence emission upon excitation at 285 nm, and far-UV CD spectral data. Fig. 5A shows the fluorescent spectral changes for SARS_NP at 0.09 mg/ml in Buffer D in the presence of different concentrations of urea at pH 9.0, and the goodness of the fitting is according to (Eq. (7)). As shown in Fig. 5A, an apparent decrease in fluorescent intensity at 340 nm was observed upon unfolding. The native SARS_NP exhibited emission λ_{max} around 333±0.5 nm, and λ_{max} of SARS_NP was found to shift to 346±1 nm when denatured by urea and GuHCl, as expected for a tryptophan exposed to solvent. The far-UV CD spectra of SARS_NP at 0.45 mg/ml in Buffer D with different concentrations of urea suggested that SARS_NP lost its secondary structures with increasing urea concentration and fully denatured at 5 M urea.

$\Delta G_u^{H_2O}$ (free energy change of thermal-induced denaturation), m and C_m (transition midpoint of chemical induced denaturation) could be calculated using (Eq. (7)) (where $\Delta G_u^{H_2O}=mC_m$), and the results were summarized in Table 2. C_m (4.29 M) and $\Delta G_u^{H_2O}$ (7.188 kcal/mol) of SARS_NP unfolding were the highest at pH 9.0. This suggests the same results as in the thermal-induced unfolding characterization that SARS_NP has the maximum conformational stability near pH 9.0. It could be also found from Table 2 that when pH became higher or lower than 9, the stability of this protein decreased as reflected by the reduced values of C_m and $\Delta G_u^{H_2O}$. The results from the urea-induced denaturation investigated by fluorescence and far-UV CD spectra are shown to be in good agreement with each other (Table 2).

As we know, urea and guanidine hydrochloride (GuHCl) are the most commonly used denaturants in the studies of protein unfolding and refolding. The equilibrium unfolding transitions induced by these two denaturants are not always similar to each other, and the difference might be more related to the ionic character for GuHCl [38]. GuHCl-induced unfolding of SARS_NP obeys the similar transition pattern as the urea-induced unfolding. However, as shown in Table 2, $\Delta G_u^{H_2O}$ obtained by GuHCl-induced unfolding is a little bigger than that by urea-induced unfolding, at pH 9.0, for example, 7.1884 kcal/mol for urea-induced unfold-

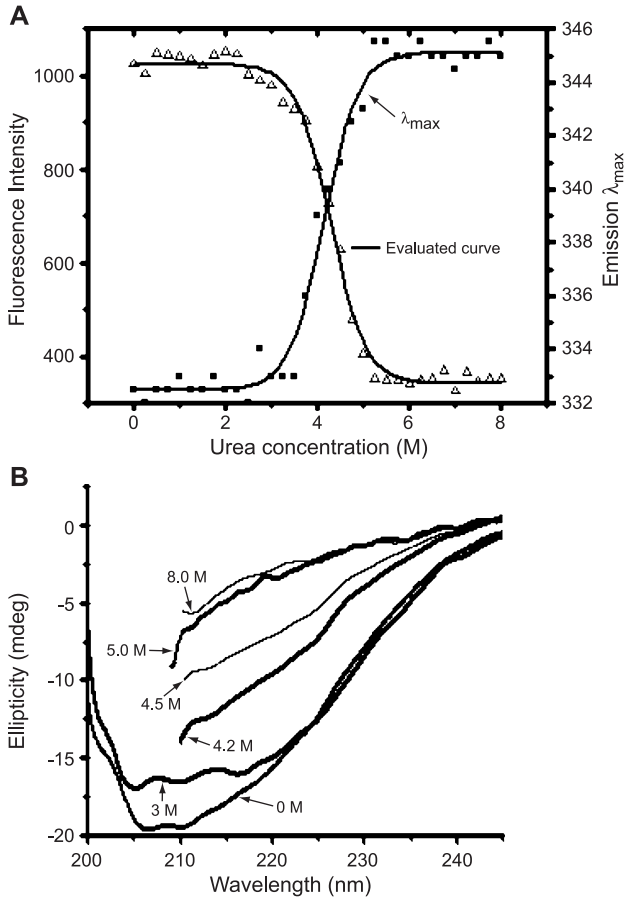

Fig. 5. Chemical denaturant-induced unfolding of SARS_NP. Fluorescent changes (A) and far-UV CD spectra at 222 nm (B) of SARS_NP (pH 9.0) in different concentrations of urea in Buffer D. The solid curves in (A) shows goodness of fitting by Eq. (7). Protein concentrations used in fluorescent experiments was at 0.09 mg/ml, and CD at 0.45 mg/ml. All samples were prepared in Buffer D and measured at 25 °C.

Table 2
Thermodynamic parameters for the chemical denaturant-induced denaturation of SARS_NP*

pH	Fluorescence						Far-UV CD (222 nm)		
	Urea			GuHCl			Urea		
	C_m (M)	m (kcal/M)	$\Delta G_u^{H_2O}$ (kcal/M)	C_m (M)	m (kcal/M)	$\Delta G_u^{H_2O}$ (kcal/M)	C_m (M)	m (kcal/M)	$\Delta G_u^{H_2O}$ (kcal/M)
6.0	2.27	1.638	3.682	1.09	3.735	4.071	2.13	1.703	3.624
7.0	2.54	1.781	4.542	1.14	4.539	5.163	2.78	1.806	5.023
8.0	3.27	1.701	5.638	1.55	3.663	5.677	3.15	1.649	5.212
9.0	4.29	1.665	7.188	2.11	3.696	7.801	4.44	1.675	7.275
10	3.56	1.794	6.392	1.77	3.669	6.486	3.61	1.825	6.412
11	3.19	1.736	5.736	1.64	3.544	5.813	3.18	1.656	5.103

* The values represent the mean of three independent sets of experiments with S.D. of less than 10%.

ing and 7.801 kcal/mol for GuHCl. Such a difference in free energy of unfolding may thus be also attributed to the ionic effect of GuHCl.

3.5. Refolding studies

Thermal-induced denaturation of SARS_NP was refolded by cooling the protein sample down to 20 °C and let to be kept at this temperature for 12 h before analyzed by fluorescence and CD measurements. We found that thermal-induced denaturation of SARS_NP is not reversible. Denatured SARS_NP in 8 M urea was refolded by diluting to lower urea concentrations and kept at 20 °C for 12 h before monitoring the λ_{max} at 25 °C. The refolding sample applied to CD was prepared by dialysis against Buffer D for 24 h and was measured at 25 °C. The results shown in Fig. 6A and B indicated that urea-induced unfolding and refolding is basically reversible.

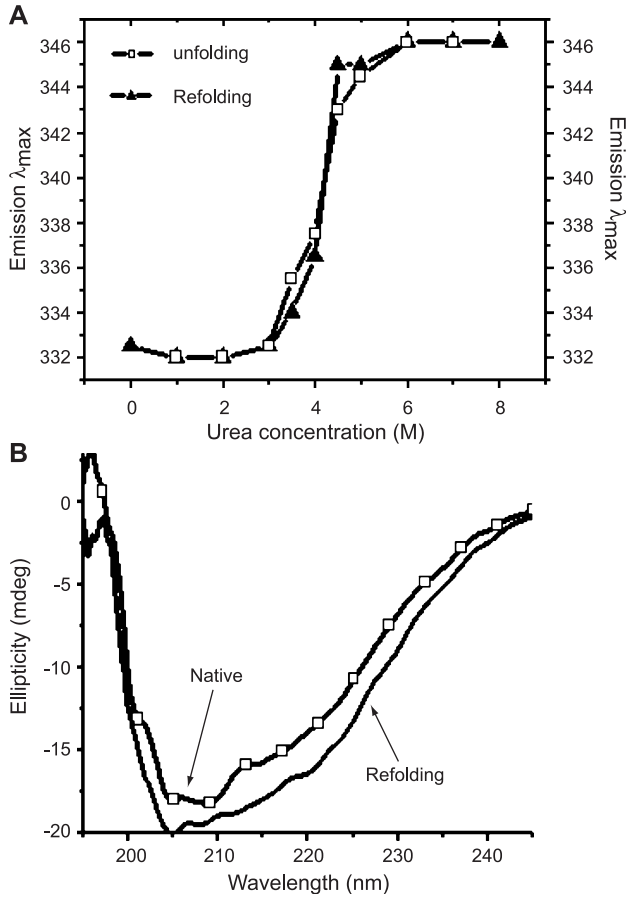

Fig. 6. Refolding studies of SARS_NP. (A) λ_{max} shifts for urea-induced unfolding and refolding courses of SARS_NP; (B) far-UV CD spectra of native and refolding SARS_NP (urea-induced unfolding). All samples were prepared in Buffer D (pH 9.0) and data were recorded at 25 °C.

In conclusion, in this work, the important biochemical and thermodynamic features of SARS_NP were characterized with the help of SPR technology, non-denatured gel electrophoresis, gel filtration in FPLC system, fluorescent and circular dichroism (CD) investigations. SARS_NP is prone to assembling itself as dimer below ~4 μM and incompact oligomer at higher concentration (over 4 μM) in the absence of genomic RNA. SARS_NP might exist in oligomer, more probably dimer, as the basic functional unit in vivo. Thermal and chemical denaturant-induced denaturations of SARS_NP are subject to the two-state transition model: NU. In addition, it is found that the dissociation of subunit and loss of SARS_NP structure are of simultaneous events. The denaturation investigation has proved that SARS_NP shows its most stable conformation near pH 9.0 with the highest $\Delta G_u^{H_2O}$ and ΔG°. The electrostatic interactions among the charge groups make a significant contribution to the conformational stability for SARS_NP. Thermal-induced unfolding and refolding are irreversible, while urea-induced unfolding of SARS_NP is nearly reversible.

Acknowledgements

The authors are grateful to the Chinese Military Medical Academy for providing the SARS_CoV (BJ01) virus. This work was supported by the State Key Program of Basic Research of China (grants 2003CB514125, 2003CB514124, 2002CB512807, 2002CB512801, 2002CB512802, and 2002CB512802), the National Natural Science Foundation of China (grants 20372069, 29725203 and 20072042), Shanghai Basic Research Project from the Shanghai Science and Technology Commission (grant 02DJ14070), the 863 Hi-Tech Program (grants 2001AA235051, 2001AA235071 and 2002AA233011), and the special programs of oppugn-

ing SARS from the Ministry of Science and Technology, Chinese Academy of Sciences, National Natural Science Foundation of China and Shanghai Science and Technology Commission.

Appendix A. Supplementary data

Supplementary data associated with this article can be found, in the online version, at doi:10.1016/j.bpc.2004.06.008.

References

[1] J.S. Peiris, C.M. Chu, V.C. Cheng, K.S. Chan, I.F. Hung, L.L. Poon, K.I. Law, B.S. Tang, T.Y. Hon, C.S. Chan, K.H. Chan, J.S. Ng, B.J. Zheng, W.L. Ng, R.W. Lai, Y. Guan, K.Y. Yuen, Clinical progression and viral load in a community outbreak of coronavirus-associated SARS pneumonia: a prospective study, Lancet 361 (2003) 1767–1772.

[2] J.S. Peiris, S.T. Lai, L.L. Poon, Y. Guan, L.Y. Yam, W. Lim, J. Nicholls, W.K. Yee, W.W. Yan, M.T. Cheung, V.C. Cheng, K.H. Chan, D.N. Tsang, R.W. Yung, T.K. Ng, K.Y. Yuen, Coronavirus as a possible cause of severe acute respiratory syndrome, Lancet 361 (2003) 1319–1325.

[3] C. Drosten, S. Gunther, W. Preiser, S. Van der Werf, H.R. Brodt, S. Becker, H. Rabenau, M. Panning, L. Kolesnikova, R.A. Fouchier, A. Berger, A.M. Burguiere, J. Cinatl, M. Eickmann, N. Escriou, K. Grywna, S. Kramme, J.C. Manuguerra, S. Muller, V. Rickerts, M. Sturmer, S. Vieth, A.D. Osterhaus, H. Schmitz, H.W. Doerr, Identification of a novel coronavirus in patients with severe acute respiratory syndrome, N. Engl. J. Med. 348 (2003) 1967–1976.

[4] T.G. Ksiazek, D. Erdman, C.S. Goldsmith, S.R. Zaki, T. Peret, S. Emery, S. Tong, C. Urbani, J.A. Comer, W. Lim, P.E. Rollin, S.F. Dowell, A.E. Ling, C.D. Humphrey, W.J. Shieh, J. Guarner, C.D. Paddock, P. Rota, B. Fields, J. DeRisi, J.Y. Yang, N. Cox, J.M. Hughes, A novel coronavirus associated with severe acute respiratory syndrome, N. Engl. J. Med. 348 (2003) 1953–1966.

[5] P.A. Rota, M.S. Oberste, S.S. Monroe, W.A. Nix, R. Campagnoli, J.P. Icenogle, S. Penaranda, B. Bankamp, K. Maher, M.H. Chen, S. Tong, A. Tamin, L. Lowe, M. Frace, J.L. DeRisi, Q. Chen, D. Wang, D.D. Erdman, T.C. Peret, C. Burns, T.G. Ksiazek, P.E. Rollin, A. Sanchez, S. Liffick, B. Holloway, J. Limor, K. McCaustland, M. Olsen_Rasmussen, R. Fouchier, S. Gunther, A.D. Osterhaus, C. Drosten, M.A. Pallansch, L.J. Anderson, W.J. Bellini, Characterization of a novel coronavirus associated with severe acute respiratory syndrome, Science 300 (2003) 1394–1399.

[6] X. Shen, J.H. Xue, C.Y. Yu, H.B. Luo, L. Qin, X.J. Yu, J. Chen, L.L. Chen, B. Xiong, L.D. Yue, J.H. Cai, J.H. Shen, X.M. Luo, K.X. Chen, T.L. Shi, Y.X. Li, G.X. Hu, H.L. Jiang, Small envelope protein E of SARS: cloning, expression, purification, CD determination, and bioinformatics analysis, Acta Pharmacol. Sin. 24 (2003) 505–511.

[7] O. Krokhin, Y. Li, A. Andonov, H. Feldmann, R. Flick, S. Jones, U. Stroeher, N. Bastien, K.V. Dasuri, K. Cheng, J.N. Simonsen, H. Perreault, J. Wilkins, W. Ens, F. Plummer, K.G. Standing, Mass spectrometric characterization of proteins from the SARS virus: a preliminary report, Mol. Cell. Proteomics. 2 (2003) 346–356.

[8] Y. Lin, X. Shen, R.F. Yang, Y.X. Li, Y.Y. Ji, Y.Y. He, M.D. Shi, W. Lu, T.L. Shi, J. Wang, H.X. Wang, H.L. Jiang, J.H. Shen, Y.H. Xie, Y. Wang, G. Pei, B.F. Shen, J.R. Wu, B. Sun, Identification of an epitope of SARS-coronavirus nucleocapsid protein, Cell Res. 13 (2003) 141–145.

[9] K. Anand, J. Ziebuhr, P. Wadhwani, J.R. Mesters, R. Hilgenfeld, Coronavirus main proteinase (3CLpro) structure: basis for design of anti-SARS drugs, Science 300 (2003) 1763–1767.

[10] B. Xiong, C.S. Gui, X.Y. Xu, C. Luo, J. Chen, H.B. Luo, L.L. Chen, G.W. Li, T. Sun, C.Y. Yu, L.D. Yue, W.H. Duan, J.K. Shen, L. Qin, T.L. Shi, Y.X. Li, K.X. Chen, X.M. Luo, X. Shen, J.H. Shen, H.L. Jiang, A 3D model of SARS-CoV 3CL proteinase and its inhibitors design by virtual screening, Acta Pharmacol. Sin. 24 (2003) 497–504.

[11] M. Von Grotthuss, L.S. Wyrwicz, L. Rychlewski, mRNA cap-1 methyltransferase in the SARS genome, Cell 113 (2003) 701–702.

[12] H.T. Yang, M.J. Yang, Y. Ding, Y. Liu, Z. Lou, Z. Zhou, L. Sun, L. Mo, S. Ye, H. Pang, G.F. Gao, K. Anand, M. Bartlam, R. Hilgenfeld, Z. Rao, The crystal structures of severe acute respiratory syndrome virus main protease and its complex with an inhibitor, Proc. Natl. Acad. Sci. U. S. A. 100 (2003) 13190–13195.

[13] K. Narayanan, A. Maeda, J. Maeda, S. Makino, Characterization of the coronavirus M protein and nucleocapsid interaction in infected cells, J. Virol. 74 (2003) 8127–8134.

[14] K. Narayanan, S. Makino, J. Maeda, C.J. Chen, Nucleocapsid-independent specific viral RNA packaging via viral envelope protein and viral RNA signal, J. Virol. 77 (2003) 2922–2927.

[15] J.C. You, C.S. McHenry, HIV nucleocapsid protein. Expression in *Escherichia coli*, purification, and characterization, J. Biol. Chem. 268 (1993) 16519–16527.

[16] L. Kuo, P.S. Masters, Genetic evidence for a structural interaction between the carboxy termini of the membrane and nucleocapsid proteins of mouse hepatitis virus, J. Virol. 76 (2002) 4987–4999.

[17] M.M. Lai, D. Cavangh, The molecular biology of coronaviruses, Adv. Virus Res. 48 (1997) 1–100.

[18] S.M. Tahara, T.A. Dietlin, C.C. Bergmann, G.W. Nelson, S. Kyuwa, R.P. Anthony, S.A. Stohlman, Coronavirus translational regulation: leader affects mRNA efficiency, Virology 202 (1994) 621–630.

[19] G.W. Nelson, S.A. Stohlman, S.M. Tahara, High affinity interaction between nucleocapsid protein and leader/intergenic sequence of mouse hepatitis virus RNA, J. Gen. Virol. 81 (2000) 181–188.

[20] T.J. Green, S. Macpherson, S. Qiu, J. Lebowitz, G.W. Wertz, M. Luo, Study of the assembly of vesicular stomatitis virus N protein: role of the P protein, J. Virol. 74 (2000) 9515–9524.

[21] M.S. Akhtar, A. Ahmad, J. Bhakuni, Guanidinium chloride- and urea-induced unfolding of the dimeric enzyme glucose oxidase, Biochemistry 41 (2002) 3819–3827.

[22] M. Surjit, B. Liu, P. Kumar, V.T. Chow, S.K. Lal, The nucleocapsid protein of the SARS coronavirus is capable of self-association through a C-terminal 209 amino acid interaction domain, Biochem. Biophys. Res. Commun. 317 (2004) 1030–1036.

[23] R. Jaenicke, R. Seckler, Protein misassembly in vitro, Adv. Protein Chem. 50 (1997) 1–59.

[24] J. Sambrook, E.F. Fritsch, T. Maniatis, Molecular Cloning, A Laboratory Manual, Cold Spring Harbor Laboratory Press, NY, 1989.

[25] H.E. Xu, M.H. Lambert, V.G. Montana, K.D. Plunket, L.B. Moore, J.L. Collins, J.A. Oplinger, S.A. Kliewer, R.T.J. Gampe, D.D. McKee, J.T. Moore, T.M. Willson, Structural determinants of ligand binding selectivity between the peroxisome proliferator-activated receptors, Proc. Natl. Acad. Sci. 20 (2003) 13919–13924.

[26] D.S. Cohen, G.J. Pielak, Stability of yeast *iso*-1-ferricytochrome *c* as a function of pH and temperature, Protein Sci. 3 (1994) 1253–1260.

[27] M.H. Brumano, E. Rogana, H.E. Swaisgood, Thermodynamics of unfolding of beta-trypsin at pH 2.8, Arch. Biochem. Biophys. 382 (2000) 57–62.

[28] R.A. Deshpande, M.I. Khan, V. Shankar, Equilibrium unfolding of RNase Rs from *Rhizopus stolonifer*: pH dependence of chemical and thermal denaturation, Biochim. Biophys. Acta 1648 (2003) 184–194.

[29] M.M. Santoro, D.W. Bolen, A test of the linear extrapolation of unfolding free energy changes over an extended denaturant concentration range1, Biochemistry 31 (1992) 4901–4907.

[30] T.L. Tellinghuisen, A.E. Hamburger, B.R. Fisher, R. Ostendorp, R.J. Kuhn, In vitro assembly of alphavirus cores by using nucleocapsid protein expressed in *Escherichia coli*, J. Virol. (1999) 5309–5319.
[31] A. Majumder, S. Basak, T. Raha, S.P. Chowdhury, D. Chattopadhyay, S. Roy, Effect of osmolytes and chaperone-like action of P-protein on folding of nucleocapsid protein of *Chandipura* virus, J. Biol. Chem. 276 (2001) 30948–30955.
[32] T. Gerelsaikhan, J.E. Tavis, V. Bruss, Hepatitis B virus nucleocapsid envelopment does not occur without genomic DNA synthesis, J. Virol. 70 (1996) 4269–4274.
[33] P. Kaukinen, V. Koistinen, O. Vapalahti, A. Vaheri, A. Plyusnin, Interaction between molecules of hantavirus nucleocapsid protein, J. Gen. Virol. 82 (2001) 1845–1853.
[34] M. Del Alamo, J.L. Neira, M.G. Mateu, Thermodynamic dissection of a low affinity protein–protein interface involved in human immunodeficiency virus assembly, J. Biol. Chem. 278 (2003) 27923–27929.
[35] S.K. Wootton, D. Yoo, Homo-oligomerization of the porcine reproductive and respiratory syndrome virus nucleocapsid protein and the role of disulfide linkages, J. Virol. 77 (2003) 4546–4557.
[36] M.V. Encinas, F.D. Gonzalez-Nilo, J.M. Andreu, C. Alfonso, E. Cardemil, Urea-induced unfolding studies of free- and ligand-bound tetrameric ATP-dependent *Saccharomyces cerevisiae* phosphoenolpyruvate carboxykinase. Influence of quaternary structure on protein conformational stability, Int. J. Biochem. Cell Biol. 34 (2002) 645–656.
[37] B. Farruggia, G.A. Pico, Thermodynamic features of the chemical and thermal denaturations of human serum albumin, Int. J. Biol. Macromol. 26 (1999) 317–323.
[38] O.D. Monera, C.M. Kay, R.S. Hodges, Protein denaturation with guanidine hydrochloride or urea provides a different estimate of stability depending on the contributions of electrostatic interactions, Protein Sci. 3 (1994) 1984–1991.